Theoretical and Experimental Study of Plate-Strengthened Concrete Columns under Eccentric Compression Loading

Lu Wang[1], Ray Kai-Leung Su[2]

Abstract

Steel jacketing has been widely used for strengthening reinforced concrete (RC) columns in the past four decades. In practice, the RC columns to be strengthened are usually subjected to eccentric pre-compressed axial loads. Until now, there have been only limited studies conducted that address the stress-lagging effects between the original column and the new jacket due to the pre-existing load. In this paper, the precambered steel plate strengthening approach, which can alleviate the stress-lagging effects, was adopted to improve the axial strength and moment capacity of the preloaded RC columns subjected to eccentric compression loading. An experimental study that involved eight specimens with different eccentricities, plate thicknesses and initial precamber displacements was conducted to examine the ductility and moment-curvature response of strengthened columns and to validate the effectiveness of this approach. A theoretical model was developed to predict the axial load capacity of the plate-strengthened columns. A comparison of the theoretical and experimental results showed that the theoretical model accurately predicted the axial load-carrying capacities of the plate-strengthened columns under eccentric compression loading.

Keywords:

Reinforced Concrete Columns; Precambered Steel Plates; Strengthening; Eccentric Loads

[1] PhD Candidate, Dept. of Civil Engineering, The Univ. of Hong Kong, Pokfulam Rd., Hong Kong, E-mail: wanglu@hku.hk

[2] Associate Professor, Dept. of Civil Engineering, The Univ. of Hong Kong, Pokfulam Rd., Hong Kong, corresponding author. E-mail: klsu@hkucc.hku.hk

Introduction

Due to the deterioration of materials and the demand for additional strength, a large number of reinforced concrete (RC) columns may need to be retrofitted or strengthened. Steel jacketing, which is executed by attaching steel plates or angles onto the concrete, has been widely used to strengthen RC structures due to the cost effectiveness and simple construction. Although a number of studies (Oey et al. 1996; Ersoy et al. 1993; Ramírez 1996; Wu et al. 2006; Fukuyama et al. 2000; Cirtek et al. 2001; Adam et al. 2007, 2008 and 2009; Giménez et al. 2009) were conducted to investigate the performance of the jacketed columns under axial compression loads, only a few considered the effects of pre-existing loads on stress-lagging between the concrete core and the new jacket. Ersoy et al. (1993), Takeuti et al. (2008) and Giménez et al. (2009) experimentally investigated the effects of pre-existing loads on the strengthening efficiency. Their test results demonstrated that the stress-lagging effects can significantly decrease the ultimate axial load capacity of the strengthened columns.

In real applications, many columns are subjected to various degrees of eccentric compression loading. The effects of RC columns strengthened by steel jackets under eccentric compression loads should be investigated. Li et al. (2009) and Garzón et al. (2011) studied the behavior of steel-caged columns under combined bending and axial loads. Their experimental results revealed that the steel strips and angles can increase the load resistance and ductility of strengthened columns. Montuori and Piluso (2009) tested thirteen RC columns strengthened by steel angles and battens under eccentric loading. Their study demonstrated that both the axial load-carrying capacity and the lateral deformability of strengthened concrete columns can be enhanced. Furthermore, they proposed a theoretical model that was able to predict the load-carrying capacity of the strengthened columns based on a kinematic mechanism. In their model, the hoops were considered simple support restraints, and the longitudinal bar was modeled as a continuous beam on simple supports that were subjected to a compressive axial load. With increasing axial load, the section of the bar between the two hoops developed a kinematic mechanism characterized by three plastic hinges. In addition, a comparison of the moment-curvature responses was performed that showed the accuracy of the model in predicting the structural response within the whole deformation range. Our companion paper (Wang and Su 2012) presented a test of nine preloaded RC columns strengthened by precambered steel plates under eccentric loading. The test results showed that precambered steel plates could actively share the existing axial loads with the original column. Stress relief in the original concrete column and post-stress developed in the steel plates can alleviate the stress-lagging and displacement incompatibility problems. Both the axial and moment capacities of strengthened columns were enhanced. The post-yield deformation was substantially increased.

In this paper, new experimental results in terms of the ductility and moment-curvature response of strengthened RC columns with precambered steel plates under eccentric compression loads are presented. A theoretical model based on elementary structure mechanics with consideration of stress-lagging effects was developed to predict the axial load-carrying capacity of plate-strengthened columns under eccentric compression loading. The accuracy of the model was verified through a comparison of the model with experimental results obtained by the authors and by Montuori and Piluso (2009).

Theoretical model

Initial Precamber

Two stainless steel rods and bolts are used to control the initial deformation of the plates and to form the required precambered profile as shown in Fig. 1. Because the bolts at both ends of the steel plates restrain the end rotations of the plates, the initial lateral displacement (v) of the precambered plate can be approximated by a cosine function (Su et al. 2011) as expressed in Eq.(1).

$$v = \frac{\delta}{2}\left[1 - \cos\left(\frac{2\pi x}{L_{rc,pl}}\right)\right] \qquad (1)$$

where δ is the initial precamber at the mid-height of the plate, $L_{rc,pl}$ is the clear height of the RC column under preloading (P_{pl}), x is the coordinate defined along the height of the column, and the subscript *pl* denotes the preloading stage. Eq. (1) satisfies the boundary conditions at both ends of the steel plates, i.e., $v = 0$ and $\frac{dv}{dx} = 0$ when $x = 0$ or $x = L_{rc,pl}$.

The difference in length of the steel plate and the RC column (Δ_L) can be evaluated by Eq. (2).

$$\Delta_L = \frac{1}{2}\int_0^{L_{rc,pl}} \left(\frac{dv}{dx}\right)^2 dx \tag{2}$$

Putting Eq. (1) into Eq. (2) gives

$$\Delta_L = \frac{(\pi\delta)^2}{4L_{rc,pl}} \tag{3}$$

Material Constitutive Laws and Simplified Stress Block Model

The stress-strain relationship of concrete in compression is represented by the parabolic relationship proposed by Hognestad et al. (1955).

$$\sigma_c = f_c^{'}\left[\frac{2\varepsilon_c}{\varepsilon_{co}} - \left(\frac{\varepsilon_c}{\varepsilon_{co}}\right)^2\right] \tag{4}$$

where $f_c^{'}$ is the concrete compressive cylinder strength, σ_c and ε_c are the stress and strain of the concrete, respectively, and ε_{co} is the concrete compressive strain corresponding to $f_c^{'}$.

Both the steel plates and steel bars are assumed to be elasto-plastic materials. In the initial elastic stage, the stress-strain models of steel plates and steel bars can be expressed as

$$\sigma_p = E_p\varepsilon_p \tag{5}$$

$$\sigma_s = E_s\varepsilon_s \tag{6}$$

where σ_p and ε_p are the stress and strain of steel plates, respectively, and σ_s, ε_s and E_s are the stress, strain and Young's modulus of the steel bars, respectively.

Collins and Mitchell (1987) noted that, for a column section with a constant width, the parabolic portion of the concrete stress distribution can be replaced by an equivalent rectangular block by introducing the stress block factors α and β as shown in Fig. 2, which can be calculated using Eq. (7) and Eq. (8).

$$\alpha = [\frac{\varepsilon_{cu}}{\varepsilon_{c0}} - \frac{1}{3}(\frac{\varepsilon_{cu}}{\varepsilon_{c0}})^2] / \beta \tag{7}$$

$$\beta = (4 - \frac{\varepsilon_{cu}}{\varepsilon_{c0}}) / (6 - \frac{2\varepsilon_{cu}}{\varepsilon_{c0}}) \tag{8}$$

Preloading stage

The preloading force is resisted by concrete and steel bars before flattening the precambered steel plates. The equilibrium equation of the RC column before flattening the plates can be obtained from the sum of the internal forces.

$$P_{pl} = \alpha\beta b(c_{pl} - 2d_b) f_c^{'} (\frac{2\varepsilon_{c,pl}}{\varepsilon_{c0}} - \frac{\varepsilon_{c,pl}^{\ 2}}{\varepsilon_{c0}^{\ 2}}) + E_{sc}A_{sc}\varepsilon_{c,pl}(\frac{c_{pl} - d^{'}}{c_{pl}}) - E_{st}A_{st}\varepsilon_{c,pl}(\frac{d - c_{pl}}{c_{pl}}) \tag{9}$$

The equation obtained from taking moments about the tension steel is

$$P_{pl}e' = \alpha\beta b(c_{pl} - 2d_b) f_c^{'} (\frac{2\varepsilon_{c,pl}}{\varepsilon_{c0}} - \frac{\varepsilon_{c,pl}^{\ 2}}{\varepsilon_{c0}^{\ 2}})(d - \frac{\beta c_{pl}}{2}) + E_{sc}A_{sc}\varepsilon_{c,pl}(\frac{c_{pl} - d^{'}}{c_{pl}})(d - d^{'}) \tag{10}$$

where b is the width of the column section as shown in Fig. 2, d and $d^{'}$ are the depths of the tension steel and the compression steel measured from extreme compression fiber, respectively, d_b is the diameter of the bolt hole, E_{sc} and E_{st} are the Young’s moduli of the compression steel bar and tension steel bar, respectively, A_{sc} and A_{st} are the total cross-sectional areas of the compression steel bars and tension steel bars, respectively, and e' is the distance between the load point and the tension steel. The depth of the compression zone (c_{pl}) and the concrete strain at extreme compression fibers ($\varepsilon_{c,pl}$) in the preloading stage can be obtained from Eqs. (7), (8), (9) and (10).

The axial stiffness of the RC column ($K_{rc,pl}$) and a steel plate (K_p) can be determined by Eq.(11) and Eq.(12), respectively.

$$K_{rc,pl} = \frac{E_c A_c}{L_{rc,pl}} \tag{11}$$

$$K_p = \frac{E_p A_p}{L_p} \tag{12}$$

where E_c and E_p are the values for the Young's moduli of concrete and steel plates, respectively, A_c is the cross-sectional area of the RC column considering the cracked section, A_p is the cross-sectional area of a steel plate and L_p is the undeformed length of the steel plate.

Post-stressing stage

When the precambered steel plates are flattened, the preloading force is resisted by concrete, steel bars and steel plates. Fig. 3 shows the lengths and deformations of the plates and the RC column at three different loading stages, i.e., the undeformed stage, the preloading stage and the post-stressing stage. By progressively tightening the bolts on both sides of the column, the precambered steel plates are gradually flattened. Due to the arching action, a post-compressive force ($P_{p,ps}$) is generated in the steel plates, and an equal magnitude de-compressive force is generated in the RC column. Using Hooke's law, the total post-stressed force provided by the plates is

$$P_{p,ps} = 2K_p\Delta_{p,ps} \tag{13}$$

where $\Delta_{p,ps}$ is the axial shortening of the steel plate while tightening the bolts when compared to the original undeformed state, and the subscript *ps* denotes the post-stressing stage.

The de-compressive force in the RC column can be written as

$$P_{p,ps} = K_{rc,pl}\Delta_{rc,ps} \tag{14}$$

where $\Delta_{rc,ps}$ is the increase in length of the RC column during the post-stressing stage, as shown in Fig. 3.

The difference in lengths of the steel plate and RC column in the preloading stage can be expressed as

$$\Delta_L = L_p - L_{rc,pl} \tag{15}$$

According to the displacement compatibility model (Fig. 3), the difference in the lengths of the steel plate and RC column in the preloading stage is equal to the sum of the axial stretching of the RC column ($\Delta_{rc,ps}$) and the axial shortening of the steel plates ($\Delta_{p,ps}$). Hence,

$$\Delta_L = \Delta_{rc,ps} + \Delta_{p,ps} \tag{16}$$

Substituting Eq. (13) and Eq. (14) into Eq. (16) gives

$$\Delta_L = \frac{K_{rc,pl} + 2K_p}{K_{rc,pl}} \Delta_{p,ps} \tag{17}$$

Putting Eq. (17) into Eq. (13), the post-compressive force in the plates can be obtained by

$$P_{p,ps} = \Delta_L \frac{2K_p K_{rc,pl}}{2K_p + K_{rc,pl}} \tag{18}$$

Meanwhile, the stress of steel plates ($\sigma_{p,ps}$) at the post-stressing stage can be expressed by

$$\sigma_{p,ps} = \frac{P_{p,ps}}{2A_p} \tag{19}$$

By considering vertical force equilibrium, the preloading force is resisted by the concrete, the steel bars and the steel plates. Hence,

$$P_{pl} = \sigma_{c,ps} A_c + \sigma_{s,ps} A_s + 2\sigma_{p,ps} A_p \tag{20}$$

where $\sigma_{c,ps}$, $\sigma_{s,ps}$ and $\sigma_{p,ps}$ are the axial stresses in the concrete, the steel bars and the steel plates in the post-stressing stage, respectively, and A_s is the total cross-sectional area of the vertical steel bars.

We assume that there is no bond slip between the steel bars and the concrete. Hence,

$$\varepsilon_{c,ps} = \varepsilon_{s,ps} \tag{21}$$

By considering the equivalent rectangular stress block, the equilibrium equation of the strengthened column can be obtained from the sum of the internal forces.

$$P_{pl} = \alpha\beta b(c_{ps} - 2d_b) f_c^{'} \left(\frac{2\varepsilon_{c,ps}}{\varepsilon_{c0}} - \frac{\varepsilon_{c,ps}^{2}}{\varepsilon_{c0}^{2}}\right) + E_{sc} A_{sc} \varepsilon_{c,ps} \left(\frac{c_{ps} - d^{'}}{c_{ps}}\right) - E_{st} A_{st} \varepsilon_{c,ps} \left(\frac{d - c_{ps}}{c_{ps}}\right) + 2A_p \sigma_{p,ps} \tag{22}$$

The equation obtained from taking moments about the tension steel is

$$P_{pl} e' = \alpha\beta b(c_{ps} - 2d_b) f_c^{'} \left(\frac{2\varepsilon_{c,ps}}{\varepsilon_{c0}} - \frac{\varepsilon_{c,ps}^{2}}{\varepsilon_{c0}^{2}}\right)\left(d - \frac{\beta c_{ps}}{2}\right) + E_{sc} A_{sc} \varepsilon_{c,ps} \left(\frac{c_{ps} - d^{'}}{c_{ps}}\right)(d - d^{'}) + 2A_p \sigma_{p,ps} d^{''} \tag{23}$$

where $d^{''}$ is the distance from the center of the compression block of the steel plate to the tension steel. The depth of the compression zone (c_{ps}) and strain of concrete ($\varepsilon_{c,ps}$) in the post-stressing stage can be obtained by solving Eqs. (7), (8), (22) and (23).

Ultimate Load Capacity

Assuming that the compression steel has been yielded, the equilibrium equation can be obtained from the sum of the internal forces.

$$P_u = \alpha\beta b(c_u - 2d_b) f_c^{'} + A_{sc} f_{scy} - A_{st} f_{st} + 2P_{pcu} - 2P_{ptu} \tag{24}$$

The equation obtained from taking moments about the tension steel is

$$P_u e' = \alpha\beta b(c_u - 2d_b) f_c^{'}(d - \frac{\beta c_u}{2}) + A_{sc} f_{scy}(d - d^{'}) + 2P_{pcu} d_{pcu} - 2P_{ptu} d_{ptu} \tag{25}$$

where f_{scy} is the compression steel yield strength, f_{st} is the stress in the tension steel, P_{pcu} and P_{ptu} are the forces defined in Fig. 4(c), and d_{pcu} and d_{ptu} are the distances from the center of force P_{pcu} and force P_{ptu} to the tension steel, respectively.

Force P_{pcu} at the ultimate load is

$$P_{pcu} = t_p f_{py} c_{pu} \tag{26}$$

where t_p is the thickness of plate, f_{py} is the yield strength of steel plate, and c_{pu} is the depth of the neutral axis measured from the extreme compression fiber of the steel plate, as shown in Fig. 4(b), which can be calculated by

$$c_{pu} = \begin{cases} h & (\text{Case1, } c_{pu} \geq h) \\ (\varepsilon_{cu} - \varepsilon_{c,ps} + \varepsilon_{p,ps}) / \phi & (\text{Case2, } c_{pu} < h) \end{cases} \tag{27}$$

where h is the width of steel plate and ϕ is the change of curvature of RC column between the post-stressing stage and the ultimate load stage, which can be expressed as

$$\phi = \phi_2 - \phi_1 = \frac{\varepsilon_{cu}}{c_u} - \frac{\varepsilon_{c,ps}}{c_{ps}} \tag{28}$$

where ϕ_1 is the curvature of RC column at the post-stressing stage and ϕ_2 is the curvature of the RC column at the ultimate load stage, as shown in Fig. 4(a).

According to the assumption of curvature compatibility between the RC column and steel plates, the force P_{ptu} is

$$P_{ptu} = t_p E_p (h - \frac{\varepsilon_{cu} - \varepsilon_{c,ps} + \varepsilon_{p,ps} - \varepsilon_{py}}{\phi}) \left[\varepsilon_{py} - (\frac{\varepsilon_{cu} - \varepsilon_{c,ps} + \varepsilon_{p,ps}}{\phi} - h)\phi \right] \tag{29}$$

The depth of the compression zone (c_u) and ultimate load-carrying capacity (P_u) can be obtained from Eqs. (7), (8), (24) to (29). If a tension failure occurs, the tension steel yields, and Eq. (24) applies with $f_{st}=f_{sty}$.

A Brief Description of Experimental Study

Because the detailed experimental procedure for preloaded RC columns strengthened with precambered steel plates subjected to eccentric loading has been presented in our companion paper (Wang and Su 2012), only a brief description of the test procedure is given in this paper. The new experimental results on ductility and moment-curvature response of eight precambered steel plate–strengthened column specimens, involving a new specimen ESC3-3, are presented.

All the tested concrete columns have the same dimensions and reinforcement arrangements. Fig. 5 shows the reinforcement and steel plate details. Specimens ESC1-1, ESC2-1 and ESC3-1 were control specimens without any strengthening measures to demonstrate the structural performance of RC columns prior to strengthening. The other five specimens were strengthened by precamber steel plates with varying initial precamber and plate thicknesses. Table 1 shows the average concrete cube and cylinder compressive strengths (f_{cu} and f_c') as well as the design parameters for each specimen. Table 2 summarizes the material properties of the steel reinforcements and steel plates. All plate-strengthened columns were subjected to preloading before the plates were flattened, which was equal to 30% of the ultimate axial load capacity of the corresponding control column. For the plate-strengthened specimens, the axial load was applied under a force control with a loading rate of 2 kN/sec. After tightening the bolts and flattening the precambered plates, the applied load was changed to a displacement control with a displacement rate of 0.5 mm/min. The test was terminated when the post-peak load reached 80% of the peak load.

Before installing the steel plates, 65 mm × 65 mm steel angles were welded to both ends of the plates, as shown in Fig. 6. The gaps between the steel angles and the concrete at the bottom and top of the steel plates were filled with an injection plaster, forming a layer of bedding between the steel angles and the concrete. The post-stress procedure described in Wang and Su (2012), which can avoid warping or buckling of the steel plates during decompression of the RC column by flattening the precambered steel plates, was adopted.

Results and Discussion

Ultimate Load Capacity and Bending Strength

Table 3 summarizes the ultimate axial load capacities of all of the specimens. Compared with the control column in each of the groups, the strengthened specimens show various degrees of strengthening from 13.9% to 64.0%. In group A, the ultimate load capacities of Specimens ESC1-2, ESC1-3 and ESC1-4 are increased by 27.1%, 64.0% and 44.6%, respectively. In group B, the ultimate load capacity of Specimen ESC2-2 is enhanced by 13.9%. In group C, the ultimate capacity of Specimen ESC3-3 is increased by 49.0%.

According to the proposed theoretical model described in the previous sections, the predicted axial load capacity (P_{pre}) of the specimens was determined by Eq. (22) and Eq. (23). During the calculations of the ultimate load capacity of the RC columns, the extreme fiber compression strain of concrete ε_{cu} was assumed to be 0.003 (Park and Paulay, 1975), and the gross sectional area of the concrete (A_c) did not include the areas of the bolt holes. The predicted axial load capacity of the specimens is presented in Table 3. Comparing the theoretical and experimental axial load capacities reveals that the proposed design procedure is generally able to conservatively estimate the actual axial load capacities of the plate-strengthened columns under eccentric compression loading with an average overestimation of 2.1%.

Due to the eccentricity of the applied axial load, a bending moment is always generated. The ultimate moment (M_u) at the mid-height of the column is composed of the primary moment (M_p), which is calculated based on the nominal eccentricity, and the secondary moment (M_s) caused by the P-Δ effect; both are summarized in Table 3. The definitions of the primary, secondary and ultimate moments can be found in Wang and Su (2012). In Group A, the secondary moment of the strengthened columns ESC1-2, ESC1-3 and ESC1-4 due to the P-Δ effect increased by 27.6%, 49.2% and 37.3%, respectively. In Group B, the secondary moment of the strengthened column due to the P-Δ effect increased by 24.9%. In Group C, the secondary moment of the strengthened column due to the P-Δ effect increased by 188.3%. It is evident that the bending moment of Specimen ESC3-3 is the largest among the eight specimens due to the largest lateral displacement and degree of eccentricity as listed in Table 3.

Deformation and Ductility

The deformability factor (λ), proposed by De Luca et al. (2011), was adopted to evaluate the deformation performance of the strengthened columns, which is defined as

$$\lambda = \Delta_f / \Delta_u \tag{30}$$

where $\varDelta_u$ is the axial shortening at the ultimate load and $\varDelta_f$ is the axial shortening at the failure load, which is equal to 75% of the ultimate load. In Group A, compared to the control column, the axial shortening at the failure load of the strengthened columns ESC1-2, ESC1-3 and ESC1-4 improved by 61.7%, 160.2% and 103.9% respectively, as shown in Fig. 7(a), and the deformability factor of the strengthened columns increased by 27.3%, 61.4% and 65.9% respectively. In Group B, compared to the control column, the axial shortening at the failure load of the strengthened column improved by 49.0%, as shown in Fig. 7(b), and the deformability factor of the strengthened column increased by 31.8%. In Group C, compared to the control column, the axial shortening at the failure load of the strengthened column improved by 222.2%, as shown in Fig. 7(c), and the deformability factor of the strengthened column increased by 93.0%. Thus, the plate thickness plays an important role in increasing the deformability of the strengthened columns, whereas the initial precamber and eccentricity do not have a substantial effect on the displacement ductility of columns.

The displacement ductility factor (η) is introduced to evaluate the ductility performance of the strengthened columns. The load-axial shortening responses of the specimens shown in Fig. 7 can be idealized as a bi-linear curve (Fig. 8). The displacement ductility factor (Su et al. 2010) is defined as the ratio of the axial shortening at peak load ($\varDelta_u$) to the notional yield displacement ($\varDelta_y$); thus,

$$\eta = \Delta_u / \Delta_y \tag{31}$$

As shown in Table 4, the displacement ductility factors range from 1.36 (for Specimen ESC2-1) to 1.94 (for Specimen ESC3-3). For each of the groups, the displacement ductility factor of the control columns was the lowest. Compared with Specimens ESC1-4 (δ = 6 mm), the displacement ductility factor of Specimens ESC1-3 (δ = 10 mm) was increased by only 3.4%. Hence, the increase in the initial precamber cannot effectively enhance the displacement ductility. Compared with Specimens ESC1-2 and ESC1-3 (e = 30 mm), the displacement ductility factors of Specimens ESC2-2 (e = 70 mm) and ESC3-3 (e = 100 mm) were increased by only 1.4% and 5.4%, respectively. Hence, the displacement ductility is not sensitive to the eccentricity of the applied load. Using thicker plates (t_p = 6 mm) for Specimen ESC1-3 instead of thinner plates (t_p = 3 mm) for Specimens ESC1-2, the displacement ductility of ESC1-3 was increased by 30.5 %. Hence, using thicker plates can effectively improve the ductility of strengthened columns.

Moment-curvature Responses

Fig. 9(a) and Fig. 9(b) show the effects of eccentricity on the moment-curvature relationship of the columns. For the specimens strengthened by 3 mm plates, the moment-curvature relationship of Specimen ESC2-2 under 70 mm eccentricity was elastic until the moment reached 13.1 kNm, which was 19.3% larger than the moment of Specimen ESC1-2 under 30 mm eccentricity. Specimen ESC2-2 failed when the curvature was $26.2\times10^{-3}\,m^{-1}$, which was 12.9% larger than that of Specimen ESC1-2. For the specimens strengthened by 3 mm plates, the moment-curvature relationship of Specimen ESC3-3 under 100 mm eccentricity was elastic until the moment reached 27.2 kNm, which was 97.1% larger than the moment of Specimen ESC1-3 under 30 mm eccentricity. Specimen ESC3-3 failed when the curvature was $38.3\times10^{-3}\,m^{-1}$, which was 13.7% larger than that of Specimen ESC1-3.

Fig. 9(c) shows the effects of the plate thickness on the moment-curvature relationship of the columns. Under the condition of 30 mm eccentricity, the moment-curvature relationship of Specimen ESC1-3 strengthened by the plates that were 6 mm thick was elastic until the moment and curvature reached 13.8 kNm and 5.8×10^{-3} m^{-1}, respectively, which were 21.1% and 99.7% larger than the moment and curvature of Specimen ESC1-2 strengthened by the plates that were 3 mm thick. Specimen ESC1-3 failed when the ultimate curvature was 32.3×10^{-3} m^{-1}, which was 38.1% larger than that of Specimen ESC1-2.

Fig. 9(d) shows the effects of the initial precamber on the moment-curvature relationship of the columns. The moment-curvature relationship of Specimen ESC1-3 with 10 mm initial precamber was elastic until the moment reached 13.8 kNm, which was 8.7% larger than that of Specimen ESC1-4 with 6 mm initial precamber. Both of them had the same curvature (5.7×10^{-3} m^{-1}) during the elastic stage. Specimen ESC1-3 failed when its curvature was 32.3×10^{-3} m^{-1}, which was 4.5% larger than that of Specimen ESC1-4. The results demonstrated that the ductility of the column was mainly affected by the plate thickness rather than the eccentricity and the initial precamber, and a larger plate thickness can provide better ductility.

Comparison with Available Experimental Results

Montuori and Piluso (2009) tested eight RC columns strengthened with steel cages subjected to eccentric compression loads. The steel cage consisted of steel angles and battens. The strengthened columns can be divided into three different types according to the function of steel angles. The ultimate capacity of the strengthened columns was evaluated using the proposed theoretical model. The stress-strain relationship of confined concrete used by Montuori and Piluso (2009) was adopted in our theoretical calculation.

Table 5 compares the ultimate load capacity presented in Montuori and Piluso (2009) with that obtained from the theoretical model. As shown in the table, all the theoretical load capacities (P_{pred}) agree well with the experimental ultimate load capacities ($P_{Mon,exp}$). The average discrepancy of $P_{Mon,exp}/P_{pred}$ is only 2%. Meanwhile, comparing the theoretical results ($P_{Mon,pred}$) proposed by Montuori and Piluso (2009) with the theoretical results obtained from our proposed model, the average discrepancy of $P_{Mon,pre}/P_{pred}$ is also 2%. Hence, the proposed theoretical model is of a similar accuracy when compared with that from Montuori and Piluso (2009).

Conclusions

The paper presents a study on the strengthening of RC columns using precambered steel plates. The theoretical and experimental findings are summarized as follows:

(1) The experimental results show that precambered plates can share the existing axial load in the original column. Stress-lagging effects can be alleviated by controlling the initial precambered profile of the steel plates.

(2) External steel plates can considerably enhance the axial strength and deformation capacity of plate-strengthened columns under eccentric compression loading.

(3) Thicker steel plates and larger initial precamber can enhance the ultimate load capacity of columns, and a larger plate thickness can also improve the axial deformation capacity and ductility of columns significantly.

(4) The bending moment capacity of a column is significantly affected by the degree of eccentricity because the larger degree of eccentricity can increase the lateral displacement at the mid-height of columns and, hence, increase the secondary moment caused by the P-Δ effect.

(5) An original theoretical model was developed based on the principles of force equilibrium and the displacement compatibility between the steel plates and the RC column. The experimental and theoretical results showed a good agreement with each other. The comparison between the available test results of Montuori and Piluso (2009) and the predicted theoretical results was also presented. This study demonstrates that the theoretical model is able to accurately predict the axial load-carrying capacity of the plate-strengthened columns under eccentric compression loading.

Acknowledgements

The research described here was supported by the Research Grants Council of the Hong Kong SAR (Project No. HKU7166/08E) and The University of Hong Kong through Small Project Funding 2010-2011.

References

Adam, J.M., Ivorra, S., Gimenez, E., Moragues, J.J., Miguel, P., Miragall, C. and Calderon, P.A. (2007). “Behaviour of axially loaded RC columns strengthened by steel angles and strips.” *Steel and Composite Structures*, 7(5), 405-419.

Adam, J.M., Gimenez, E., Calderon, P.A., Pallarés, F.J. and Ivorra, S. (2008). “Experimental study of beam-column joints in axially loaded RC columns strengthened by steel angles and strips.” *Steel and Composite Structures*, 8(4), 329-342.

Adam, J.M., Ivorra, S., Pallares, F.J., Gimenez, E. and Calderon, P.A. (2008). “Column-joint assembly in RC columns strengthened by steel caging.” *Proc. ICE - Structures and Buildings*, 161(6), 337-348.

Adam, J.M., Ivorra, S., Pallares, F.J., Gimenez, E. and Calderon, P.A. (2009). “Axially loaded RC columns strengthened by steel caging: Finite element modeling.” *Construction and Building Materials*, 23(6), 2265-2276.

Adam, J.M., Ivorra, S., Pallares, F.J., Gimenez, E. and Calderon, P.A. (2009). “Axially loaded RC columns strengthened by steel caging.” *Proc. ICE - Structures and Buildings*, 162(3), 199-208.

Cirtek, L. (2001). “RC columns strengthened with bandage – experimental programme and design recommendations.” *Construction and Building Materials*, 15(8), 341–349.

Collins, M.P. and Mitchell, D. (1987) *Prestressed Concrete Structures*, Prentice Hall, Englewood Cliffs.

De Luca, A., Nardone, F., Matta, F., Nanni, A., Liqnola, G. and Prota, A. (2011). “Structural evaluation of full-scale FRP-confined reinforced concrete columns.” *Journal of Composites for Construction*, 15(1), 112-123.

Ersoy, U., Suleiman, R. and Tankut, T. (1993). “Behavior of jacketed columns.” *ACI Structural Journal*, 90(3), 288-293.

Frangou, M., Pilakoutas, K. and Dritsos, S. (1995). “Structural repair/strengthening of RC Columns.” *Construction and Building Materials*, 9(5), 259-266.

Fukuyama, H. and Sugano, S. (2000). “Japanese seismic rehabilitation of concrete buildings after the Hyogoken-Nanbu Earthquake.” *Cement and Concrete Composites*, 22(1), 59-79.

Garzón-Roca, J., Adam, J.M. and Calderón, P.A. (2011). “Behaviour of RC columns strengthened by steel caging under combined bending and axial loads.” *Construction and Building Materials*, 25(5), 2402-2412.

Garzón-Roca, J., Ruiz-Pinilla, J., Adam, J.M. and Calderón, P.A.(2011). “An experimental study on steel-caged RC columns subjected to axial force and bending moment.” *Engineering Structures*, 33(2), 580-590.

Giménez, E., Adam, J.M., Ivorra, S. and Calderón, P.A. (2009). “Influence of strips configuration on the behaviour of axially loaded RC columns strengthened by steel caging and strips.” *Materials and Design*, 30(10), 4103-4111.

Giménez, E., Adam, J.M., Ivorra, S., Moragues, J.J., and Calderón, P.A. (2009). “Full-scale testing of axially loaded RC columns strengthened by steel angles and strips.” *Advances in Structural Engineering*, 12(2), 169-181.

Hognestad, E., Hanson, N., McHenry, D. (1955). “Concrete stress distribution in ultimate strength design.” *ACI Structural Journal*, 52(6), 455-479.

Li, J., Gong, J. and Wang, L. (2009). “Seismic behavior of corrosion-damaged reinforced concrete columns strengthened using combined carbon fiber-reinforced polymer and steel jacket.” *Construction and Building Materials*, 23(7), 2653-2663.

Montuori, R. and Piluso, V. (2009). “Reinforced concrete columns strengthened with angles and battens subjected to eccentric load.” *Engineering Structures*, 31(2), 539-550.

Oey, H.S. and Aldrete, C.J. (1996). “Simple method for upgrading an existing reinforced-concrete structure.” *Practice Periodical on Structural Design and Construction*, 1(1), 47-50.

Ramírez, J.L. (1966). “Ten concrete column repair methods.” Construction and Building Materials, 10(3), 195-202.

Su, R.K.L., Cheng, B., Wang, L., Siu, W.H. and Zhu, Y. (2011). “Use of bolted steel plates for strengthening of reinforced concrete beams and columns”, *The IES Journal Part A: Civil & Structural Engineering*, 4(2), 55-68.

Su, R.K.L., Siu, W.H. and Smith, S.T. (2010). “Effects of bolt-plate arrangements on steel plate strengthened reinforced concrete beams.” *Engineering Structures*, 32(6), 1769-1778.

Su, R.K.L., and Wang, L. (2012). “Axial strengthening of preloaded rectangular concrete columns by precambered steel plates.” *Engineering Structures*, (Article in press).

Park, R., and Paulay, T. (1975) *Reinforced Concrete Structures*, John Wiley & Sons, New York.

Takeuti, R.A., de Hanai, J.B. and Mirmiran, A. (2008). “Preloaded RC columns strengthened with high-strength concrete jackets under uniaxial compression.” *Materials and Structures*, 41(7), 1251-1262.

Wang, L. and Su, R.K.L. (2012). “Experimental investigation of preloaded RC columns strengthened with precambered steel plates under eccentric compression loading.” *Advances in Structural Engineering*, (Article in press).

Wu, Y.F., Liu, T. and Oehlers, D.J. (2006). “Fundamental principles that govern retrofitting of reinforced concrete columns by steel and FRP jacketing.” *Advances in Structural Engineering*, 9(4), 507-533.

Table 1. Summary of strengthening details

Group	Specimen	f_{cu} (MPa)	f'_c (MPa)	E_c (GPa)	L_{rc} (mm)	e (mm)	t_p (mm)	δ (mm)	P_{pl} (kN)
[A]	ESC1-1	31.3	25.6	23.8	600	30	-	-	-
	ESC1-2	31.9	25.8	23.9	600	30	3	10	101
	ESC1-3	31.6	25.9	23.9	600	30	6	10	101
	ESC1-4	32.7	26.1	24.0	600	30	6	6	101
[B]	ESC2-1	33.3	27.8	24.8	600	70	-	-	-
	ESC2-2	32.0	25.7	23.8	600	70	3	10	63
[C]	ESC3-1	29.7	24.2	23.1	600	100	-	-	-
	ESC3-3	32.6	26.5	24.2	600	100	6	10	43

Table 2. Material properties of reinforcements and steel plates

Steel Plate		
Thickness	f_{yp}(MPa)	E_p (GPa)
3 mm	301	215
6 mm	327	219

Reinforcement bars		
Specimen	f_y(MPa)	E_s (GPa)
T10	497	198
T12	516	198
R6	464	186
R8	437	187

Table 3. Comparison of the theoretical and experimental results

Group	Specimen	ζ_u (mm)	M_p (kN m)	M_s (kN m)	M_u (kN m)	P_{exp} (kN)	P_{pred} (kN)	P_{exp}/P_{pred}
[A]	ESC1-1	5.51	10.08	1.85	11.93	336	329	1.02
	ESC1-2	5.53	12.81	2.36	15.17	427	390	1.09
	ESC1-3	5.01	16.53	2.76	19.29	551	545	1.01
	ESC1-4	5.23	14.58	2.54	17.12	486	471	1.03
[B]	ESC2-1	9.62	14.63	2.01	16.64	209	208	1.01
	ESC2-2	10.55	16.66	2.51	19.17	238	227	1.05
[C]	ESC3-1	10.11	14.30	1.45	15.75	143	143	1.00
	ESC3-3	17.36	24.10	4.18	28.28	213	222	0.96

Note: **P_{exp} is the test result, P_{pred} is the predicted result.**

Table 4. Summary of deformability and ductility factors

Group	Specimen	Δ_y (mm)	Δ_u (mm)	Δ_f (mm)	λ	η
[A]	ESC1-1	0.71	0.97	1.28	1.32	1.37
	ESC1-2	0.87	1.23	2.07	1.68	1.41
	ESC1-3	0.85	1.56	3.33	2.13	1.84
	ESC1-4	0.67	1.19	2.61	2.19	1.78
[B]	ESC2-1	0.28	0.38	0.49	1.29	1.36
	ESC2-2	0.30	0.43	0.73	1.70	1.43
[C]	ESC3-1	0.14	0.21	0.27	1.29	1.50
	ESC3-3	0.18	0.35	0.99	2.83	1.94

Table 5. Comparison of ultimate load capacities from Montuori and Piluso (2009) and the present proposed theoretical model

Specimen	$P_{Mon,exp}$ (kN)	$P_{Mon,pred}$ (kN)	P_{pred} (kN)	$P_{Mon,exp}/P_{pred}$	$P_{Mon,pred}/P_{pred}$
A-R1	513.95	527.02	507.08	1.01	1.04
B-R1a	703.23	683.62	683.38	1.03	1.03
B-R1b	662.71	649.75	656.56	1.01	0.99
C-R1	498.74	495.15	480.55	1.04	1.03
D-R1	545.19	553.24	528.23	1.03	1.05
D-R2	568.98	583.22	563.18	1.01	1.04
D-R3	483.63	453.84	462.86	1.04	0.98
E-R1	713.24	713.80	705.28	1.01	1.01
Mean	-	-	-	1.02	1.02

Note: **$P_{Mon,exp}$ is the test result and $P_{Mon,pred}$ is the predicted result, both from Montuori and Piluso (2009).**

A List of Figure Captions

Figure 1. The configuration of the proposed strengthening method

Figure 2. Stress-block factors

Figure 3. Lengths and deformations of RC column and steel plates at various loading stages

Figure 4. Strain distribution and calculation; (a) Concrete strain distribution; (b) Steel plate strain distribution; (c) Steel plate stress distribution in the theoretical calculation

Figure 5. Reinforcement and precambered steel plates; (a) RC details; (b) Steel plate details

Figure 6. Joint at the end of precambered steel plates; (a) Anchor bolts details; (b) Steel angle details

Figure 7. Load-axial shortening curves; (a) Group A; (b) Group B; (c) Group C

Figure 8. Definition of displacement ductility factor

Figure 9. Moment-curvature responses of columns; (a) t_p=3 mm, δ=10 mm; (b) t_p=6 mm, δ=10 mm; (c) e=30 mm, δ=10 mm; (d) t_p=6 mm, e=30 mm

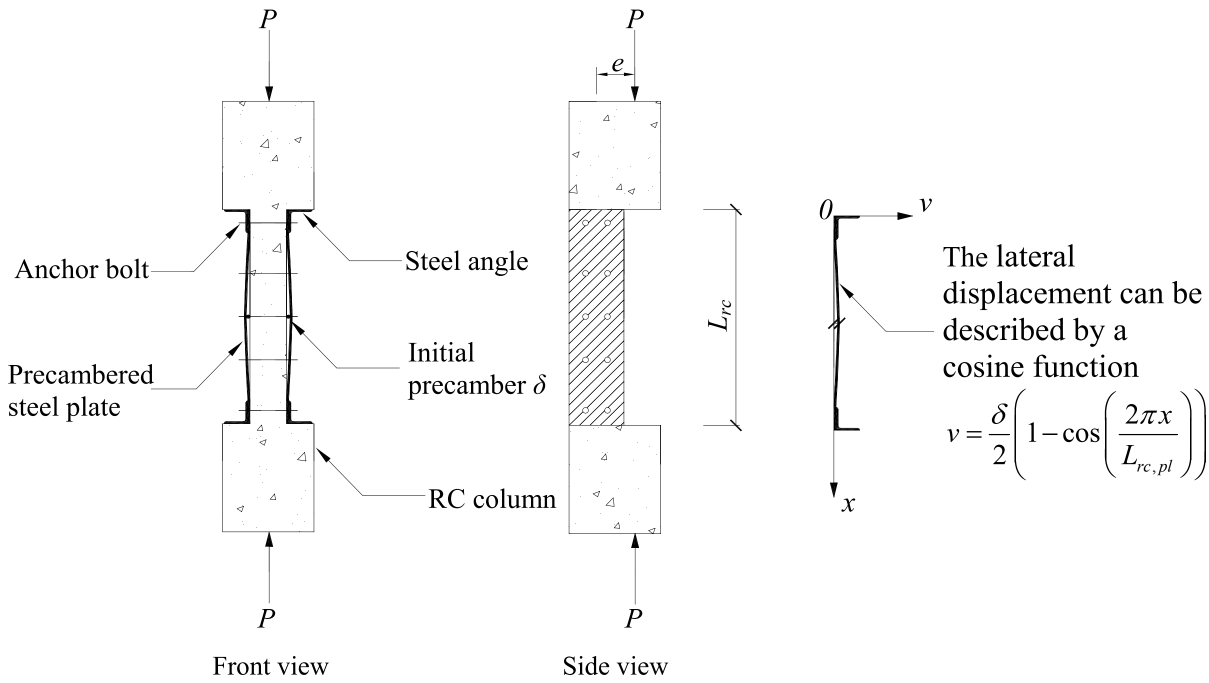

Fig. 1. The configuration of the proposed strengthening method

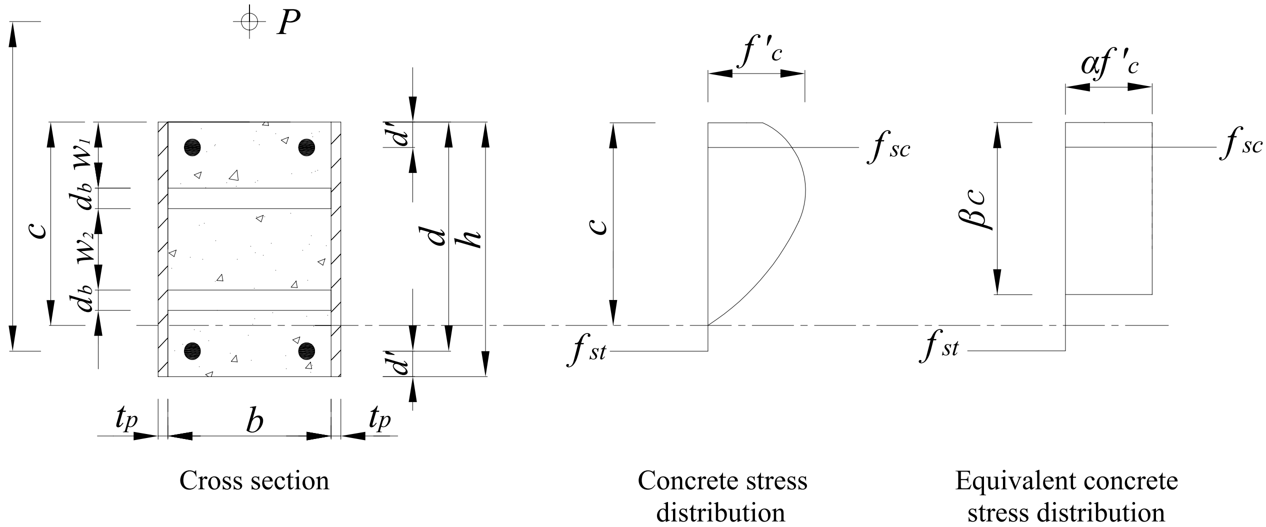

Fig. 2. Stress-block factors

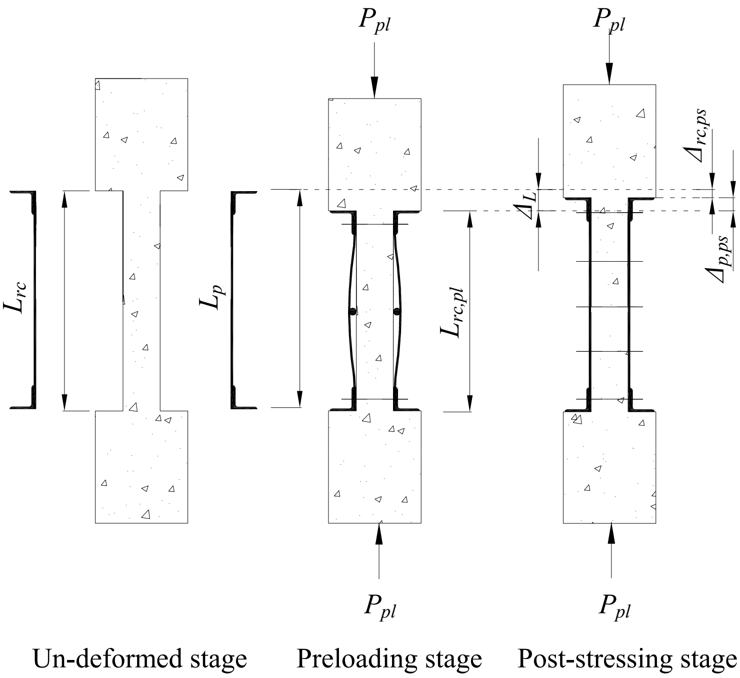

Fig. 3. Lengths and deformations of RC column and steel plates at various loading stages

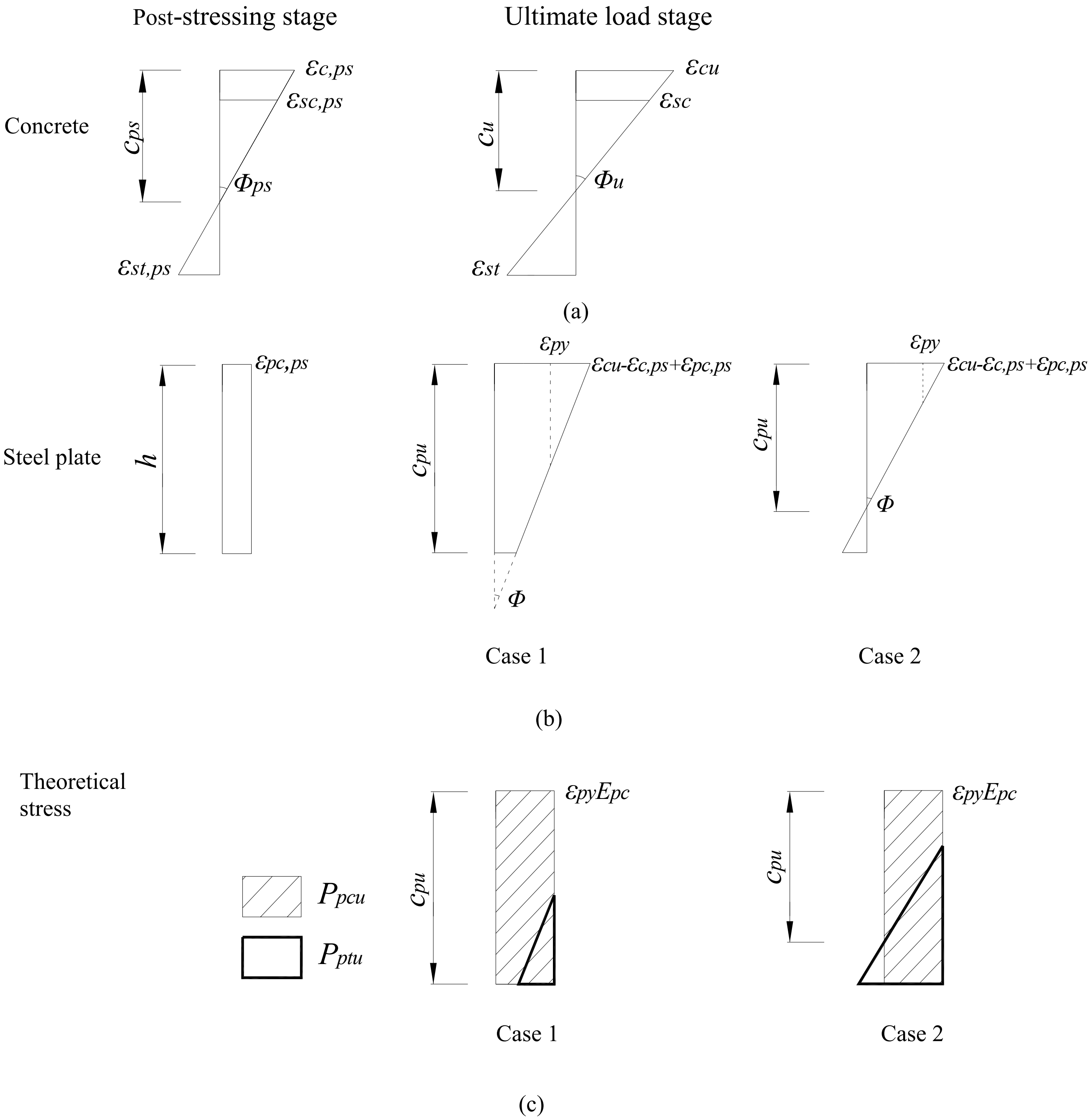

Fig. 4. Strain distribution and calculation; (a) Concrete strain distribution; (b) Steel plate strain distribution; (c) Steel plate stress distribution in the theoretical calculation

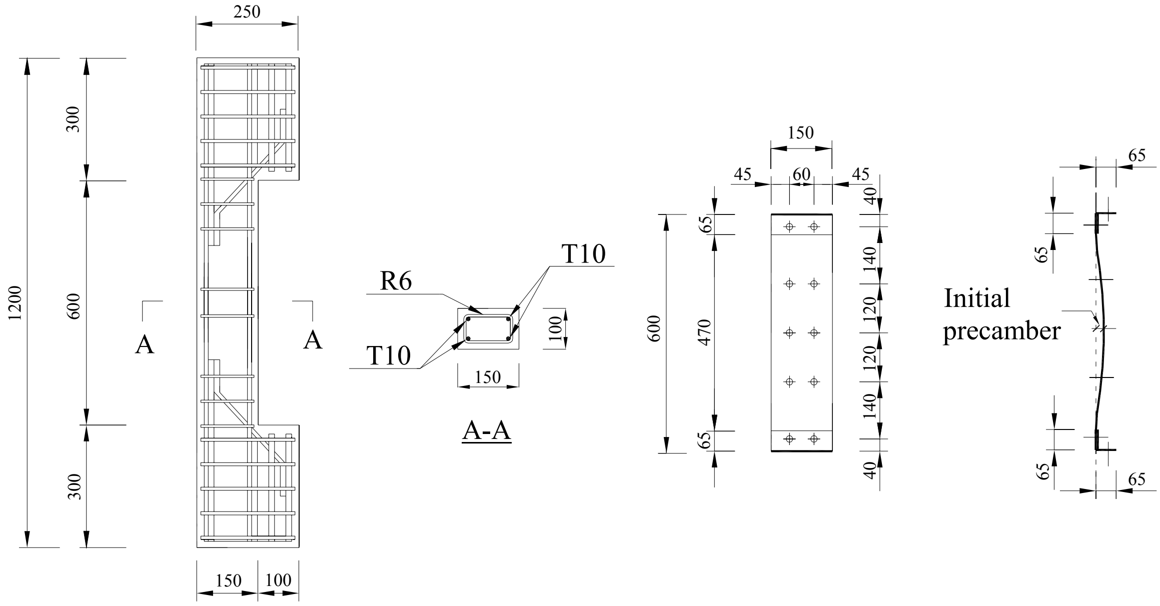

(a) (b)

Fig. 5. Reinforcement and precambered steel plates; (a) RC details; (b) Steel plate details

(a) (b)

Fig. 6. Joint at the end of precambered steel plates; (a) Anchor bolts details; (b) Steel angle details

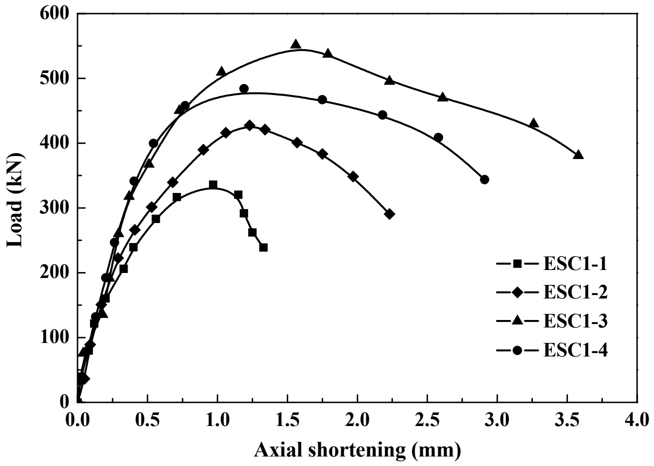

(a)

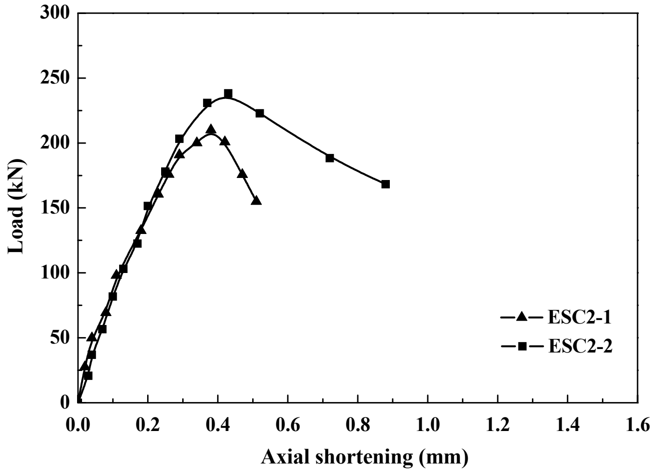

(b)

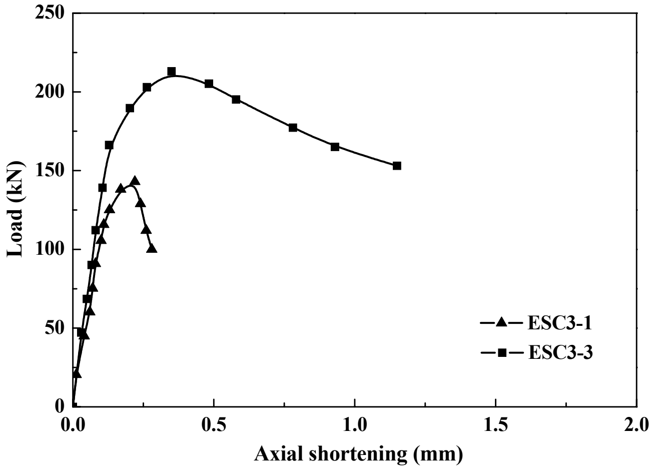

(c)

Fig. 7. Load-axial shortening curves; (a) Group A; (b) Group B; (c) Group C

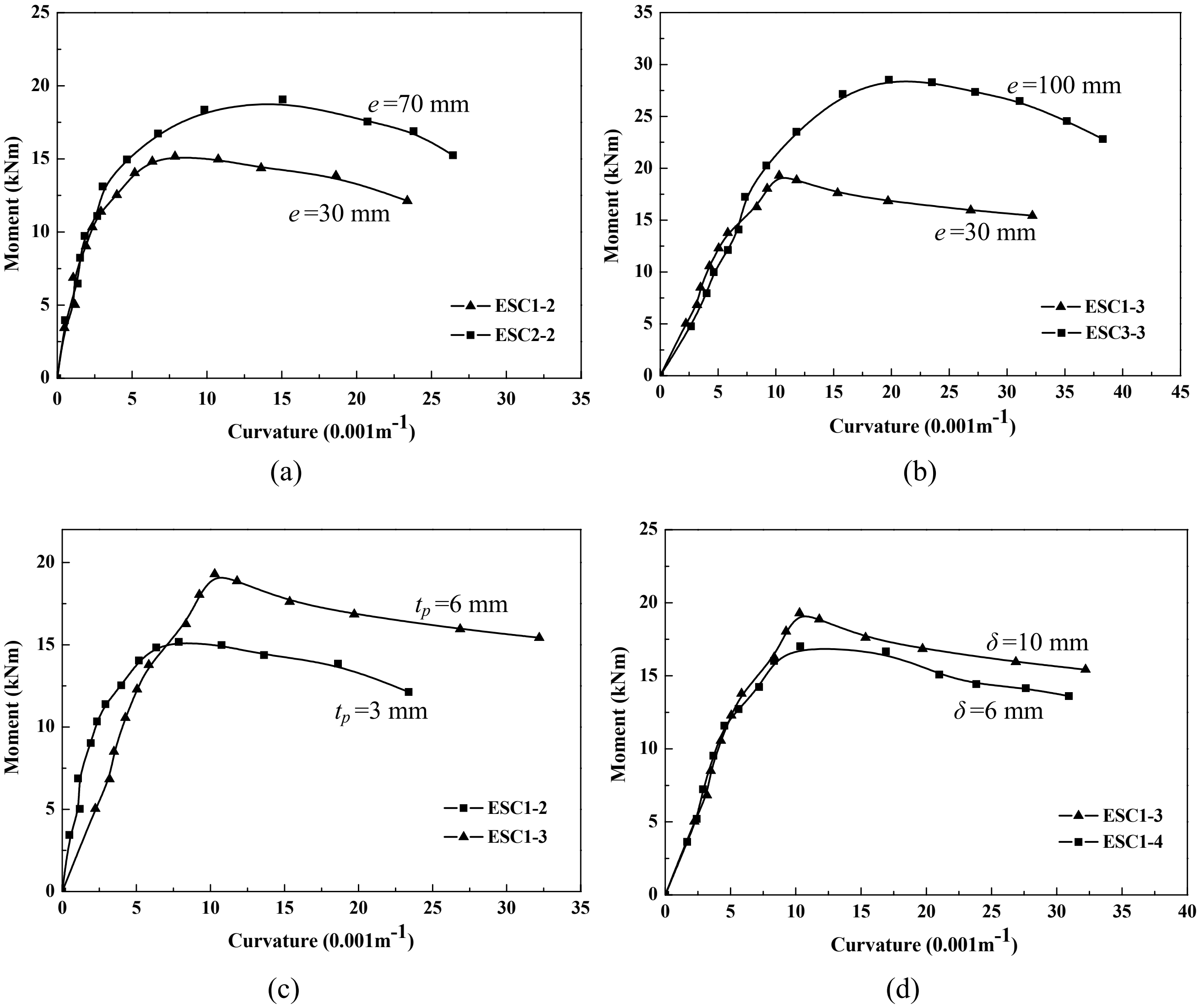

Fig. 8. Moment-curvature responses of columns; (a) t_p=3 mm, δ=10 mm; (b) t_p=6 mm, δ=10 mm; (c) e=30 mm, δ=10 mm; (d) t_p=6 mm, e=30 mm